PCCP

View Online / Journal Homepage
Dynamic Article Links

Cite this: DOI: 10.1039/c2cp40565b

www.rsc.org/pccp

PAPER

O_2 induced Cu surface segregation in Au–Cu alloys studied by angle resolved XPS and DFT modelling

Edgar Völker,[ab] Federico J. Williams,[a] Ernesto J. Calvo,[a] Timo Jacob[c] and David J. Schiffrin*[b]

Received 23rd February 2012, Accepted 28th March 2012
DOI: 10.1039/c2cp40565b

Surface segregation effects on polycrystalline Au–Cu alloys ($Au_{0.80}Cu_{0.20}$, $Au_{0.85}Cu_{0.15}$ and $Au_{0.90}Cu_{0.10}$) were studied at room temperature by angle resolved XPS (ARXPS) and density functional theory (DFT) before and after exposure to O_2. Au surface enrichment was found as predicted from calculations showing that this process is energetically favourable, with a segregation energy for Au in a Cu matrix of -0.37 eV atom^{-1}. Surface enrichment with Cu was observed after exposure to O_2 due to its dissociative adsorption, in agreement with DFT calculations that predicted an energy gain of -1.80 eV atom^{-1} for the transfer of Cu atoms to a surface containing adsorbed oxygen atoms, thus leading to an inversion in surface population.

1. Introduction

The increase of CO_2 concentration in the atmosphere constitutes a major environmental challenge that has triggered an increased interest in studies focussed on the elimination or the conversion of this molecule. Reduction of CO_2 has been investigated as a possible route for its use as a raw material to produce useful products, as a way of energy storage or for the production of low molecular weight organic compounds to participate in carbon neutral cycles.[1,2] The original work by Hori *et al.*[3] demonstrated that Cu can act as an unusually active electrocatalyst leading to the production of alcohols, acids and C-1 to C-5 hydrocarbons.[4,5] The product distribution is strongly dependent on electrode surface treatment. Performance is complicated by the ease of oxidation of copper surfaces and one of the strategies to achieve control on surface oxidation is to alloy copper with gold, since Au and Cu are known to yield single-phase solid solutions over the whole compositional range.[6] Au–Cu alloys have also attracted considerable interest as catalysts for many gas-phase reactions such as CO oxidation, propene epoxidation and selective oxidation of benzyl alcohol to yield benzaldehyde.[7]

The electrocatalytic properties of alloys depend on surface composition, which is, in general, different from that in the bulk due to differences in the surface segregation energy of alloy constituents, a question that has been extensively discussed.[8,9] The binary alloy system Au–Cu is a typical example of an alloy displaying surface segregation phenomena that has been investigated both experimentally[10–13] and theoretically.[14–16] Theoretical studies give a qualitative description of surface enrichment even though only considering that one of the components of the alloy is a single atom (the guest) embedded in a matrix of atoms of the other alloy component (the host). In consequence, these calculations do not take into account guest-guest interactions, which are of fundamental importance for predicting surface composition.

Chemisorption from the gas or solution phase onto the alloy surface can change the equilibrium concentration thus resulting in chemisorption-induced surface segregation, which in some cases can lead to an inversion of the composition of the segregated atoms.[13,17,18] In electrochemical experiments, adsorbate-induced changes in composition have been recently demonstrated and importantly, shown to result in changes of the oxygen reduction mechanism for Au-Pd alloys.[19] In this type of experiments, adsorbed oxygen resulting from the partial anodic oxidation of the alloy can play a fundamental role in establishing the reaction pathway to either water or hydrogen peroxide. The study of surface segregation when the alloy is in contact with a condensed phase is not simple and for this reason, segregation phenomena induced by oxygen adsorption from the gas phase has been investigated in the present work.

The purpose of this work was to study the segregation properties of polycrystalline Au–Cu alloys ($Au_{0.80}Cu_{0.20}$, $Au_{0.90}Cu_{0.10}$ and $Au_{0.85}Cu_{0.15}$) in UHV at room temperature. The effect of exposure of the first two alloys mentioned to an atmosphere of pure O_2 was investigated employing angle resolved XPS (ARXPS) and the experimental observations of adsorbate induced segregation were analysed using density functional theory (DFT) modelling.

[a] *Departamento de Química Inorgánica, Analítica y Química-Física, INQUIMAE-CONICET, Facultad Ciencias Exactas y Naturales, Pabellón 2, Ciudad Universitaria, Buenos Aires, Argentina C1428EHA*
[b] *Chemistry Department, University of Liverpool, Liverpool, UK L69 7ZD*
[c] *Institute of Electrochemistry, Ulm University, Albert-Einstein-Allee 47, D-89081 Ulm, Germany*

2. Experimental

2.1 Alloy preparation and surface treatment

Au–Cu polycrystalline alloys were prepared from high purity base metals (3 mm diameter Au and Cu rods 99.9985%, Premion®, and 99.999%, Puratronic®, respectively, Alfa Aesar, UK). The rods were cleaned in boiling acetone and cut and weighed to obtain the correct Au/Cu fraction. They were then placed in alumina crucibles and heated in a tube furnace (CTF 12/75/700, Carbolite, UK) under 10% H_2/90% Ar (BOC gases, UK) at 1100 °C for 6 h. The samples were left to cool in the reducing atmosphere of the furnace and extracted only when they reached room temperature. The samples thus obtained were flattened into panels of 1 cm diameter and 0.5 mm thickness, then cleaned in boiling acetone and polished with 1200 and 2400 abrasive paper and finally with 9, 3, 1, 0.3 and 0.05 μm alumina slurries (Buehler, Germany); the samples were rinsed with copious amounts of Milli-Q water (Millipore, USA) and sonicated in Milli-Q water between each polishing step. The materials thus prepared were analyzed by X-ray diffraction (PANalytical X'pert PRO Multi-Purpose Diffractometer, Co $K\alpha_1$ radiation), to ensure that alloys were formed.

2.2 X-ray photoelectron spectroscopy

XPS measurements were performed in a SPECS UHV (SPECS, Germany) spectrometer system equipped with a 150 mm mean radius hemispherical electron energy analyzer and a nine channeltron detector (base pressure $< 5 \times 10^{-10}$ mbar). XP spectra were acquired at a constant pass energy of 20 eV using a Mg-Kα (1253.6 eV) source operated at 12.5 kV and 20 mA. Measurements were performed with a variable detection angle (see below ARXPS technique) with respect to the sample surface normal. The binding energies quoted are referred to the Au $4f_{7/2}$ emission at 84.0 eV. Alloy samples were cleaned by Ar^+ sputtering until no contaminants were observed on their surfaces. The sample and support were grounded and no charge compensation was necessary as indicated by the absence of differential charging features, *e.g.*, low binding energy tails. Atomic ratios were calculated from the integrated intensities of core level signals after corrections for instrumental and photoionisation atomic sensitivity factors.[20,21]

2.3 ARXPS measurements and analysis

XPS measurements were performed as a function of detection angle defined as the angle between the electron analyzer and the normal to the surface. Thus, the information collected at high detection angles has a higher surface sensitivity than that at smaller detection angles. The angles used (θ) were 5, 30, 45, 60, 68 and 75°. To convert the angle-dependent XPS data into depth profiles, a maximum entropy approach was used as described in detail elsewhere.[22–24] Only a brief outline will be given here.

Consider a sample from which a set of angle resolved XP spectra has been acquired. If the sample consists of j slabs that contain i elements at concentration $c_{j,i}$, the total intensity detected at an angle θ for element i can be expressed as:

$$I_i(\theta) = \sum_j I_{j,i}(\theta) \qquad (1)$$

for which

$$I_{j,i}(\theta) = s_i c_{j,i} \exp\left[\frac{-z\cos(\theta)}{\lambda_i}\right]^{j-1} \qquad (2)$$

where z is the thickness of each slab; s_i and λ_i are the sensitivity factor and attenuation length for each element, respectively.

The procedure to estimate concentration profiles requires the optimisation of two quantities, a minimisation of the least squares deviation from estimated trial functions and the maximisation of an entropy term corresponding to the minimum information content consistent with the experimental data, as discussed by Livesey and Smith.[23]

For each trial profile for each element, the sum of the squares of the errors (χ^2) was calculated according to:

$$\chi_1^2 = \sum_\theta \frac{(I_i^{calc}(\theta) - I_i^{obs}(\theta))}{\sigma_1^2(\theta)} \qquad (3)$$

where $\sigma_i(\theta)$ is the standard deviation due to experimental noise at an angle θ. This expression must be minimized while maximizing the entropy term S:

$$S = \sum_{j,i} c_{j,i} - c_{j,i}^o - c_{j,i} \ln\left[\frac{c_{j,i}}{c_{j,i}^o}\right] \qquad (4)$$

where $c_{j,i}^o$ is the initial estimate for the concentration of species i at slab j. In ARXPS, the strategy is to reconstruct the profile from a data set consisting of intensity measurements containing some instrumental noise. The solution to this problem is the reconstruction that satisfies the data but contains the minimum amount of structure necessary to do so, as it is not desirable to fit the details of the noise in the data. The required solution is therefore the concentration profile that has the minimum information content (*i.e.* maximum entropy), consistent with the data.[23]

The two conditions can be met simultaneously by minimizing the quantity $Q = 0.5\chi^2 - \alpha S$, where α is a regularisation constant that gives appropriate weights to the minimization of the squared errors (χ) and the information content (S).[24] A large value of α would result in overly smoothed profiles, while a small value would lead to data overfitting (*i.e.* fitted to the noise). The calculated profiles were obtained by carrying out the above calculation in an MS Excel spreadsheet using the SOLVER subroutine.[25]

2.4 O_2 dosing

Scheme 1 shows a diagram of the experimental arrangement employed. The sample was transferred from the main analysis chamber ($p \approx 5 \times 10^{-10}$ mbar) to the loading chamber ($p \approx 5 \times 10^{-8}$ mbar) with a mechanical arm and then transferred to the gas-dosing chamber *via* a second mechanical arm at 90 degrees from the first. Once there, the valve connecting the loading with the gas dosing chamber was closed and O_2 (99.99%, INDURA, Argentina) was fed, thus exposing the sample to O_2. The turbo pump connected to the loading chamber was switched off and as atmospheric pressure was reached, pure N_2 was fed into the loading chamber closing simultaneously the flow of O_2 to the gas chamber. The valve connecting both chambers was then opened; the sample transferred to the loading chamber and the pump was switched on again. Once the pressure reached $\approx 5 \times 10^{-8}$ mbar, the sample was transferred back into the main chamber for measurements.

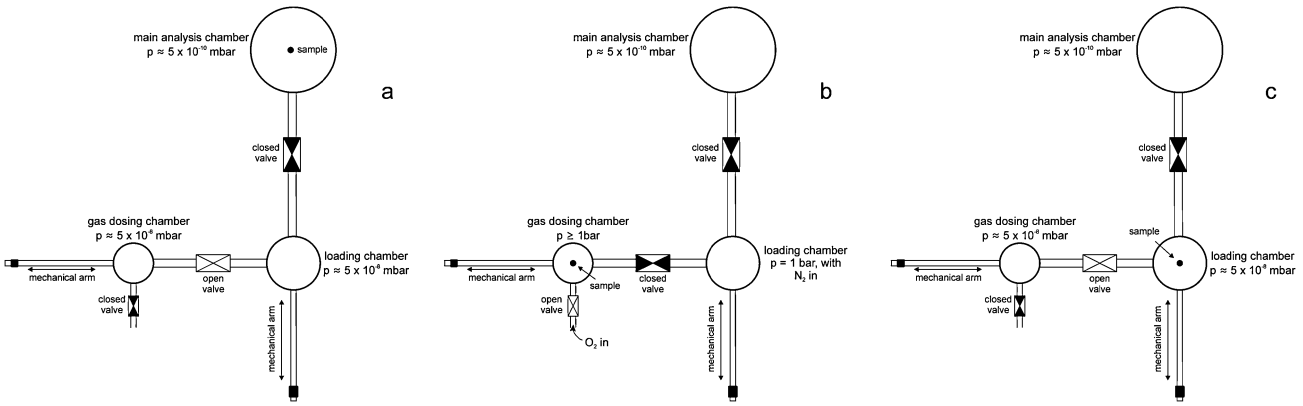

Scheme 1 Scheme of the XPS experimental setup for O_2 dosing. (a) Setup used when measuring XPS spectra. During this procedure, the loading and gas dosing chambers are connected and have the same base pressure of $\approx 5 \times 10^{-8}$ mbar. (b) During O_2 dosing, pure O_2 is admitted to a pressure above 1 bar, the pump connected to the loading chamber is switched off and when atmospheric pressure is reached, it automatically doses N_2 into it. (c) The O_2 dosing valve is closed, the sample is transferred back into the loading chamber and the pump is switched back on, emptying both the loading and gas dosing chambers down to $\approx 5 \times 10^{-8}$ mbar. When this pressure is reached, the sample is transferred back into the main analysis chamber to be studied.

The whole operation took approximately 15 min; most of the time was taken to pump empty the loading chamber. The O_2 exposure time was 5 min for all samples studied.

3. DFT calculations

DFT calculations were performed with SeqQuest,[26] a periodic DFT code with localized basis sets represented by linear combinations of contracted Gaussian functions (here at the "double-ζ plus polarization"-level). The PBE-GGA exchange–correlation functional was employed in tandem with standard (non-local) norm-conserving pseudopotentials. Integrations in reciprocal space were performed with a Brillouin zone sampling of 9×9 k-points per 1×1 unit cell. All surfaces were represented by six-layer slabs where the lowest two layers were fixed to the calculated bulk structure while all remaining layers were allowed to optimize freely their geometry (up to less than 0.1 eV $Å^{-1}$).

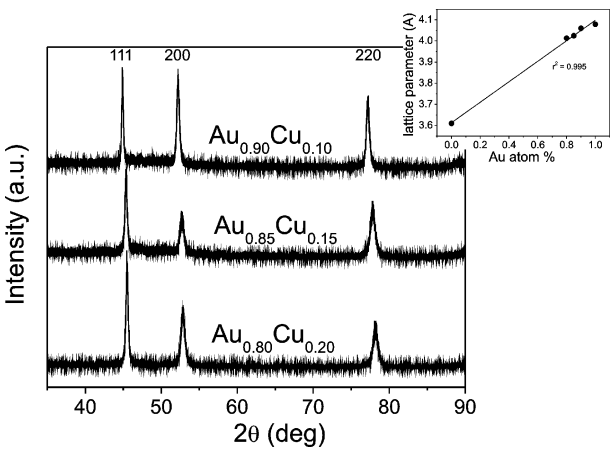

Fig. 1 X-ray diffraction spectra of the Au/Cu alloys studied. The inset shows the corresponding Vegard's law plot.

4. Results

4.1 Characterisation of the alloys

Fig. 1 shows the X-ray diffraction spectra of the $Au_{0.80}Cu_{0.20}$, $Au_{0.85}Cu_{0.15}$ and $Au_{0.90}Cu_{0.10}$ alloys. No individual reflections for the alloying elements are observed, indicating that the samples obtained were solid solutions. In addition, the expected shifts for the Au reflections predicted from Vegard's law[27] are observed in these results (See inset to Fig. 1) for increasing concentration of Cu. The lattice parameters were calculated[28] for the three reflections observed and the average values obtained were 4.013 ± 0.006 Å for $Au_{0.80}Cu_{0.20}$, 4.025 ± 0.006 Å for $Au_{0.85}Cu_{0.15}$ and 4.060 ± 0.005 Å for $Au_{0.90}Cu_{0.10}$. These lie between those of Au (4.079 Å) and Cu (3.610 Å).

4.2 ARXPS of Au/Cu alloys

Fig. 2 shows the Cu and Au atomic compositions for $Au_{0.80}Cu_{0.20}$, $Au_{0.85}Cu_{0.15}$ and $Au_{0.90}Cu_{0.10}$ as a function of XPS detector angle. The relative compositions were calculated taking into account the sensitivity factors for Au and Cu from the literature.[20,21] The solid lines in Fig. 2 show the best fits using the concentration-gradient model with maximum entropy regularisation described in Section 2.3.[22–24]

The insets to Fig. 2 show the dependence of the Au 4f and Cu $2p_{3/2}$ XP signals on detection angle (the spectra are shifted for clarity). The Au and Cu compositions were calculated from the ratio of these two XP signals and their corresponding relative atomic sensitivity factors.[21] The Au 4f signals show a clear increase in intensity as the detection angle is increased, whereas the Cu $2p_{3/2}$ signals decrease demonstrating surface enrichment in Au for the three alloys studied. As expected, the measured Au and Cu compositions tend towards their nominal bulk values as the detection angle is decreased. The Cu $2p_{3/2}$ XP signal is seen at a binding energy of 932.4 eV, which is ascribed to metallic Cu with no contributions from copper oxides, as can be seen from the negligible O 1s signal observed (see later Fig. 4).

Fig. 3 presents the corresponding depth profiles for the three samples obtained from fitting the data as described in Section 2.3, showing the surface segregation of Au on these alloys, as predicted from theoretical calculations.[14,15]

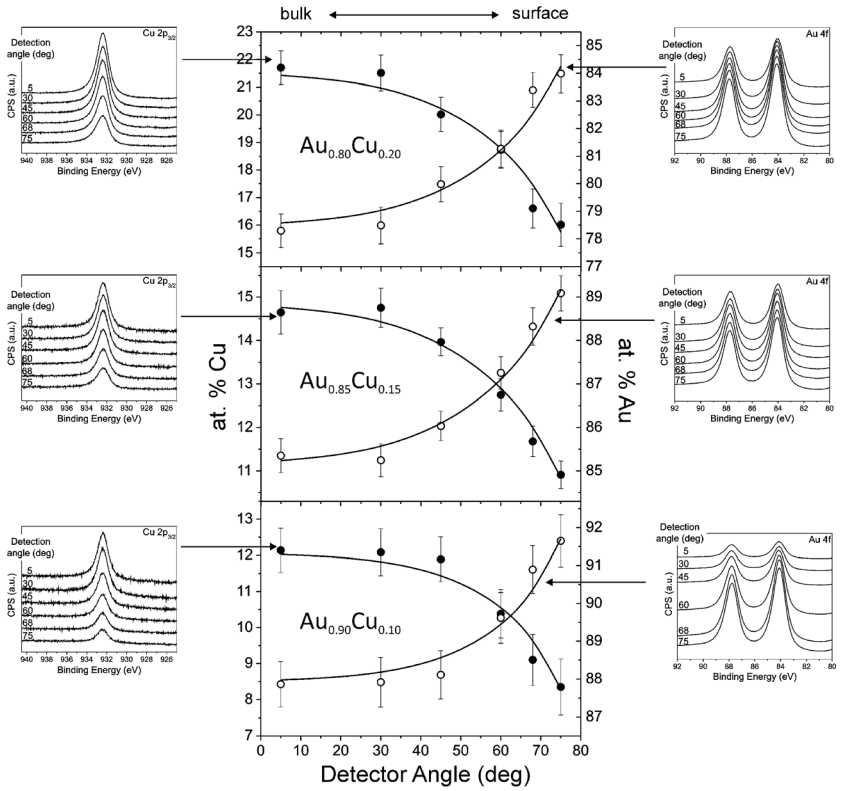

Fig. 2 Cu (filled circles, left) and Au atomic % (open circles, right) calculated from the XPS data obtained as a function of detector angle for the three polycrystalline Au–Cu alloys studied ($Au_{0.80}Cu_{0.20}$–top, $Au_{0.85}Cu_{0.15}$—middle and $Au_{0.90}Cu_{0.10}$–bottom). The lines correspond to the best fit obtained using a concentration-gradient model with maximum entropy regularisation.[22,24] Insets: Au 4f and Cu $2p_{3/2}$ signals for each sample (The spectra are shifted for clarity).

4.3 Effects of exposure to O_2

Fig. 4 shows the O 1s signal for the $Au_{0.80}Cu_{0.20}$ and $Au_{0.90}Cu_{0.10}$ samples before and after exposure to O_2 (see experimental Section 2.4) taken at a detection angle of 75°. It was found that the surface sensitivity and signal intensity were optimal at this angle.

Immediately after sample cleaning and before exposure to O_2, both samples showed almost no presence of O, except for a small signal at ≈532 eV, which is probably due to minor organic contamination remaining on the sample. After exposure to O_2, the O 1s XP signal increased dramatically with a peak centred at ≈530.9 eV, which is attributed to adsorbed atomic O.[29] It is noticeable that for the $Au_{0.80}Cu_{0.20}$ alloy with a higher Cu content than the other sample, the signal increase is more pronounced, demonstrating the role of Cu in the alloy for enhancing O chemisorption.

Fig. 5 and 6 show the elemental surface compositions calculated from the Au 4f and Cu $2p_{3/2}$ signals at different detection angles for the $Au_{0.80}Cu_{0.20}$ and $Au_{0.90}Cu_{0.10}$ alloys before and after O_2 exposure, as well as their corresponding concentration fits.[22–24] A clear change in surface composition is observed after exposure to O_2. The surface of both samples becomes enriched with Cu, with an inversion of surface composition for Cu, an effect which is more pronounced in the $Au_{0.80}Cu_{0.20}$ alloy, showing a total change of approximately 18% compared with 12% for the $Au_{0.90}Cu_{0.10}$ alloy. It should be noted that the results in Fig. 5 correspond to a two-element system before O adsorption, whereas a three-element system is present after adsorption. The results at high take-off angles clearly show the large segregation induced by O adsorption. This effect was further analysed by calculating the corresponding concentration profiles.

The depth profiles calculated with the model used predict changes that correspond to topmost surface layers properties. It is useful to compare the results shown in Fig. 6 with the atomic radii of Au and Cu, 1.442 and 1.278 Å, respectively.[30] Considering these atomic sizes, it can be seen from Fig. 6 that the main influence of O adsorption is to modify the composition of the first few layers of the alloys.

Surface roughness of the sample can play an important role in the depth profiles measured.[31,32] Great care was taken during the manipulation and polishing of the samples and sputtering was kept to a minimum until almost no C contamination was detected, so as to minimise the influence of roughness on the ARXPS results. The experimental data used to calculate the depth profiles is obtained, however, from *ratios* of the XP signals for the different elements, therefore diminishing the influence of roughness in the profiles calculated.

4.4 DFT results

In order to verify the reversal of surface segregation caused by oxygen adsorption, density functional theory (DFT) calculations were performed for two different systems, clean and oxygen-covered (θ = 1.0 ML) surfaces. Place exchange energies for Cu were calculated using slab geometries. The calculations were carried

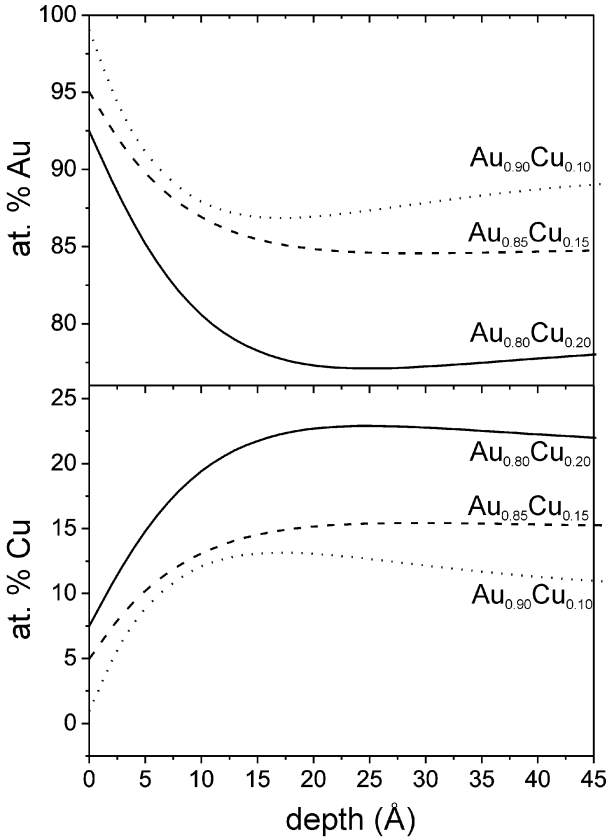

Fig. 3 Depth profiles for Au (top) and Cu (bottom) for the three alloys studied: (full line): $Au_{0.80}Cu_{0.20}$; (dashed line): $Au_{0.85}Cu_{0.15}$; (dotted line): $Au_{0.90}Cu_{0.10}$. The profiles were converted from the best fit to the ARXPS data shown in Fig. 2.

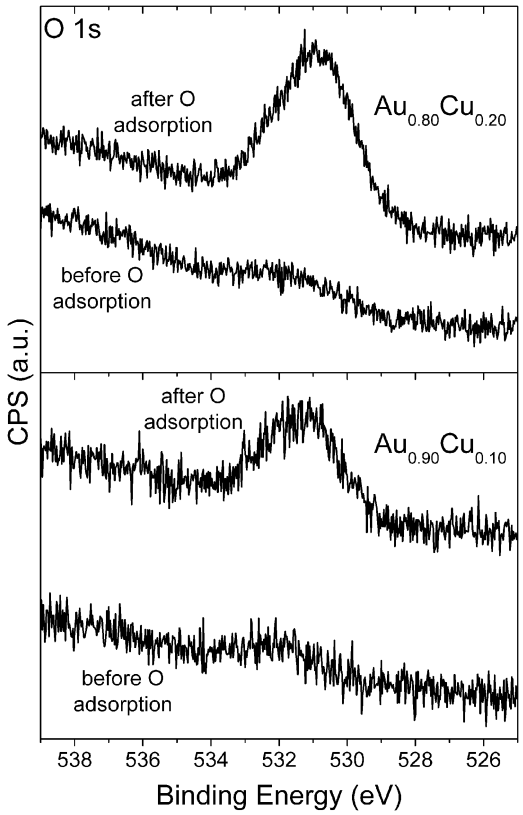

Fig. 4 O 1s XP signal for $Au_{0.80}$ $Cu_{0.20}$ (above) and $Au_{0.90}$ $Cu_{0.10}$ (below) samples, before and after exposure to 1 bar of O_2, taken at a detection angle of 75 deg with respect to surface normal. The spectra have been shifted for comparison.

out on Au(111) surfaces when either the first or the second layer had been fully exchanged with Cu atoms, thus representing preferential segregation of either Au or Cu to the surface.

Fig. 7 shows schematically the structures modelled. In the absence of adsorbates, the calculated energy for a monolayer of adsorbed Cu to segregate to subsurface sites was -0.37 eV atom^{-1} (Process I $\rightarrow$ II in Fig. 7, negative energies indicate an overall energy gain). This shows that Au is preferentially situated at the surface. The dissociative adsorption of 1.0 ML of oxygen on a gold terminated slab requires 0.45 eV per oxygen atom (Process II $\rightarrow$ III in Fig. 7; all the values have been referenced to $\frac{1}{2}$ O_2(g)). This process is endothermic since the formation of an adsorbed layer by dissociation of gaseous O_2 is considered here and the adsorption energy of oxygen on gold is relatively low. Process III $\rightarrow$ IV corresponds to the place exchange of surface Au atoms by Cu with oxygen attached to Cu, resulting in an energy change of -1.80 eV atom^{-1}. This large value is certainly sufficient to induce almost any atom exchange at the surface resulting, therefore, in the composition and segregation changes due to the adsorption of oxygen, as observed experimentally (see Fig. 6).

5. Discussion

In agreement with DFT calculations (Process I $\rightarrow$ II in Fig. 7), the data in Fig. 2 and 3 show that in vacuum, the surface is enriched with Au for the alloys studied. The DFT calculations show a segregation energy of -0.37 eV atom^{-1} for Au atoms on the surface. There is previous experimental evidence for this result, both for polycrystalline[10,12,33] and single crystal alloys.[10,11,13] Similar conclusions have been previously reported from calculations for this system, with energy values of -0.34 and -0.17 eV atom^{-1}.[14,15] Surface enrichment by Au has also been predicted from Monte Carlo simulations[34] and for a 55 atom cluster, for which the energy gain is -0.47 eV atom^{-1}.[16] It is important to notice that many of these theoretical calculations are simplifications of real systems, since they consider only guest-host structures, but they do not include guest-guest interactions, although the results obtained from them provide guidelines for the expected segregation behaviour. The present DFT calculations offer a broader picture because interactions between all types of atoms (host-host, host–guest, guest-guest) are considered.

The binding energy of Cu $2p_{3/2}$ for all samples studied at all detection angles before exposure to O_2 was 932.4 eV (Fig. 2). This binding energy is ascribed to metallic Cu with no contribution from copper oxides since the O 1s XP signal before O_2 exposure at approximately 532 eV (see Fig. 4), is very small and can be attributed to minor organic contamination remaining after sputtering. This was confirmed by the small residual C 1s peak (less than 1% of the total Au 4f + Cu 2p signals). The O 1s XP signal did not increase as the detection angle was decreased, *i.e.* as deeper layers were probed. Thus, the small amount of O detected was present on the surface and not in the bulk alloy.

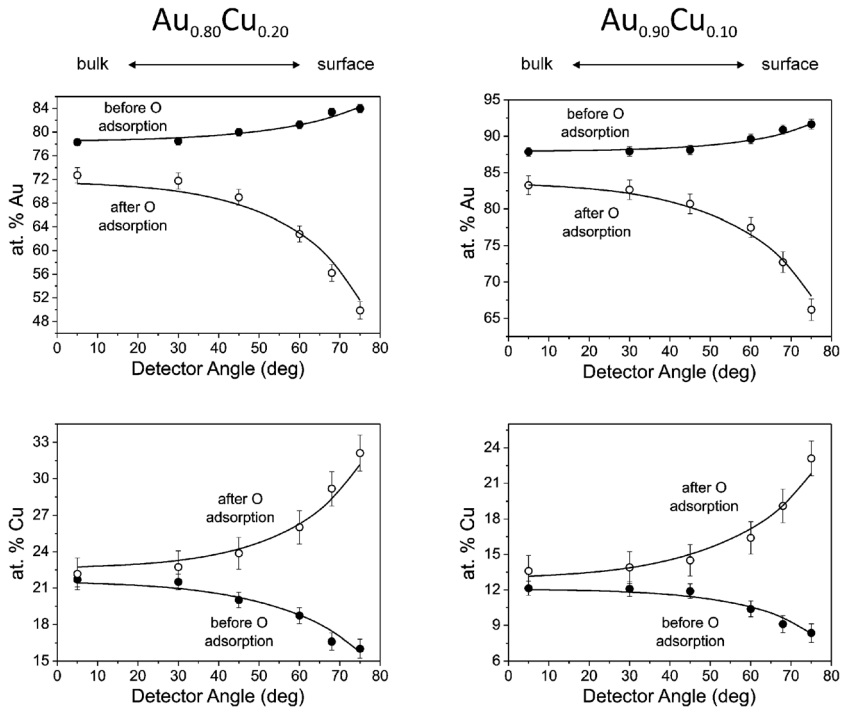

Fig. 5 Comparison of atomic Au % (top) and Cu % (bottom) for the $Au_{0.80}Cu_{0.20}$ (left) and $Au_{0.90}Cu_{0.10}$ (right) samples before (filled circles) and after (open circles) exposure to 1 bar of pure O_2. The lines show the best fit obtained using a concentration-gradient model with a maximum entropy method.[22,24]

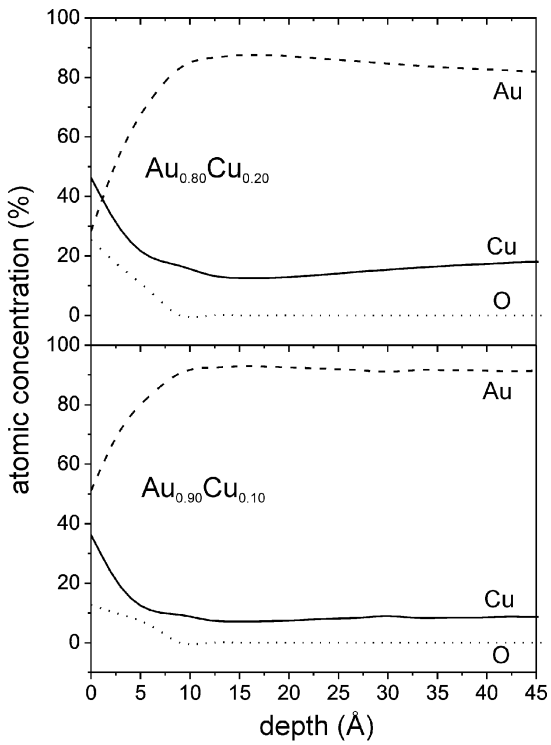

Fig. 6 Depth profiles for a $Au_{0.80}Cu_{0.20}$ alloy (top) and $Au_{0.90}Cu_{0.10}$ (bottom). The profiles were converted from the best fit to the ARXPS data shown in Fig. 5.

After exposure to O_2, the O 1s XP spectra taken at a detection angle of 75° increase and the binding energy shifts to 530.9 eV. These changes are assigned to the adsorption of

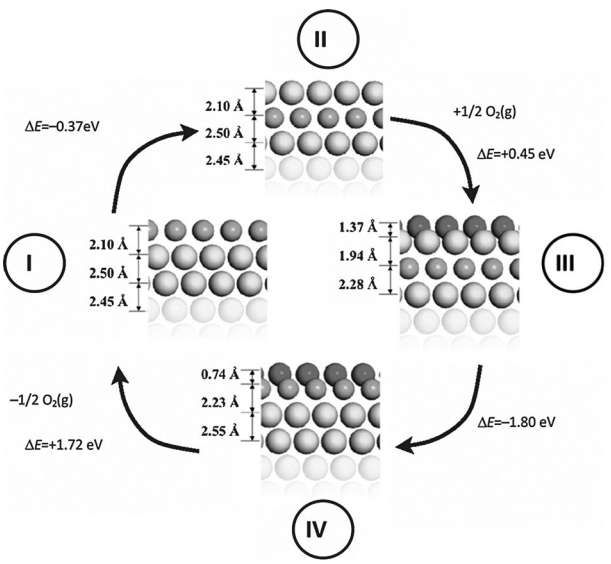

Fig. 7 Schematic illustration of oxygen-induced surface segregation. While the clean particle (top) shows Au surface segregation, adsorption of oxygen very much favours binding to Cu (bottom). The energy differences and oxygen binding energies, referenced to molecular O_2, are obtained by DFT calculations (see text).

O atoms on the surface.[29] From the DFT calculations above, if the surface remained unchanged, oxygen adsorption on Au would be very unfavourable (0.45 eV $atom^{-1}$, process II → III in Fig. 7). Surface reorganization leading to enrichment by Cu atoms takes place due to the energetically much more favourable O binding to Cu than to Au atoms (Process III → IV in Fig. 7). In consequence, the gain in energy of −1.80 eV $atom^{-1}$ resulting

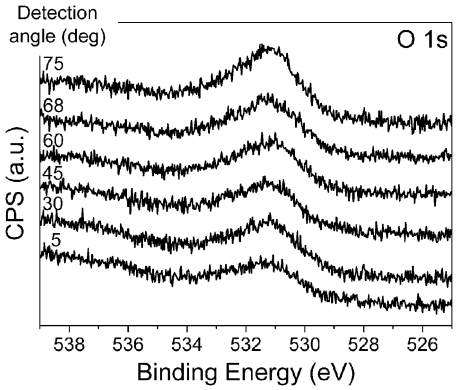

Fig. 8 XP O 1s spectra for $Au_{0.80}Cu_{0.20}$ sample after being exposed to O_2, taken at different detection angles. The spectra have been shifted for comparison.

from the transfer of Cu atoms to the surface, leads to a significant surface enrichment by Cu. Although the present calculations have only considered full monolayers, due to the very large energy gain, a similar behaviour with lower Cu surface concentrations is expected. These qualitative studies indicate that surface species showing a strong anisotropy and selectivity for binding to the different alloy constituents are capable of altering profoundly the surface composition.

ARXPS results for the O 1s signal after exposure to O_2 correspond to surface adsorbed O, as can be seen in Fig. 8 for the $Au_{0.80}Cu_{0.20}$ sample. This signal exhibits only a small increase as the detection angle increases, demonstrating that most of the O detected is present at the sample surface.

The change in surface composition due to oxygen adsorption is clearly demonstrated from the XPS results in Fig. 5 and 6, where the inversion of population of surface atoms from Au- to Cu-enriched is very noticeable. This effect is more marked for an alloy with a higher concentration of Cu. Although the percentual surface Cu concentration increase is similar for both samples (about 26%), there is a higher concentration of adsorbed O on the surface of the $Au_{0.80}Cu_{0.20}$ alloy (25%) than for the $Au_{0.90}Cu_{0.10}$ alloy (13%). In consequence, the Au surface concentration decreases for both alloys.

A slight increase in Cu population due to O adsorption was previously observed by Okada *et al.*[35] at the other extreme of Cu concentrations from that investigated here, for a Cu_3Au alloy. There is also some additional theoretical evidence for the phenomena observed.[36] The ratio between the O 1s and Cu $2p_{3/2}$ peak areas taken at a detection angle of 75° for both samples studied after exposure to O_2 gives an estimate of the O surface coverage. Not surprisingly, the coverage is larger for $Au_{0.80}Cu_{0.20}$ ($\sim$0.75 ML) than for $Au_{0.90}Cu_{0.10}$ ($\sim$0.6 ML). Similar results for the specific surface enrichment triggered by adsorbates have been obtained for Au-Pd alloys, where the presence of H or CO can induce the displacement of Pd atoms from the bulk to the surface;[18,37] and for nanoalloys where migration of Pd atoms to the surface is observed on applying potentials that result in the adsorption of oxygenated species.[19] In addition, surface rearrangements have been observed for Pt-Co nanoalloys in contact with CO.[38] Pt binds CO more strongly than Co, leading to the formation of a Pt skin, which disappears on CO removal and resulting in a repopulation of the surface with Co.[39]

Conclusions

We have shown both experimentally (ARXPS) and theoretically (DFT) that for polycrystalline Au–Cu alloys in vacuum, surface enrichment by Au at room temperature is observed. When these samples were exposed to an O_2 atmosphere, the Cu surface compositions were inverted due to O adsorption. The large changes in surface composition detected indicate that experiments in a condensed phase will not necessarily preserve the bulk alloy properties and in particular, the adsorption of oxygen species at different applied potentials in electrochemical experiments will determine the electrocatalytic properties of these alloys due to the profound changes in surface composition induced by adsorbates.[19] Thus, the present work indicates that during (electro-) catalytic reactions that involve adsorbed oxygen species, the Au–Cu alloy system might not remain rigid, but continuously change its surface composition as previously discussed for the Pd-Au system as an example of a "breathing" catalyst, *i.e.*, a surface alloy where fast atomic exchange processes driven by changes in segregation energies resulting from adsorption can take place.[18] It is expected that the phenomena observed is a general property of gold-transition metal alloys for which specific segregation of alloy components would be observed.[19]

Acknowledgements

The authors gratefully acknowledge funding by the European Union through the Marie Curie Initial Training Network ELCAT, Proposal No. 214936-2, 2008-2012.

References

1 G. A. Olah, A. Goeppert and G. K. S. Prakash, *J. Org. Chem.*, 2009, **74**, 487–498.
2 R. W. Dorner, D. R. Hardy, F. W. Williams and H. D. Willauer, *Energy Environ. Sci.*, 2010, **3**, 884–890.
3 Y. Hori, K. Kikuchi and S. Suzuki, *Chem. Lett.*, 1985, 1695–1698.
4 M. Gattrell and N. Gupta, *J. Electroanal. Chem.*, 2006, **594**, 1–19.
5 Y. Hori, A. Murata and R. Takahashi, *J. Chem. Soc., Faraday Trans. 1*, 1989, **85**, 2309–2326.
6 M. Hansen and K. Anderko, *Constitution of Binary Alloys*, McGraw Hill, New York, 1958.
7 C. L. Bracey, P. R. Ellis and G. J. Hutchings, *Chem. Soc. Rev.*, 2009, **38**, 2231–2243.
8 *Surface segregation and related phenomena*, ed. P. A. Dowben and A. Miller, CRC Press, Boca Raton Fl, 1990.
9 J. du-Plessis, *Solid State Phenom.*, 1990, **11**, 1–113.
10 J. M. McDavid and S. C. F. Jr, *Surf. Sci.*, 1975, **52**, 161–173.
11 M. J. Sparnaay and G. E. Thomas, *Surf. Sci.*, 1983, **135**, 184–198.
12 W. Losch and J. Kirschner, *J. Vac. Sci. Technol.*, 1978, **15**, 1541–1548.
13 S. Nakanishi, N. Fukuoka, K. Kawamoto, K. Umezawa, Y. Teraoka and K. Nakahigashi, *Surf. Sci.*, 1991, **247**, L215–L220.
14 A. V. Ruban, H. L. Skriver and J. K. Nørskov, *Phys. Rev. B: Condens. Matter*, 1999, **59**, 15990–16000.
15 A. U. Nilekar, A. V. Ruban and M. Mavrikakis, *Surf. Sci.*, 2009, **603**, 91–96.
16 L. Wang and D. D. Johnson, *J. Am. Chem. Soc.*, 2009, **131**, 14023–14029.
17 S. Nakanishi, K. Kawamoto, N. Fukuoka and K. Umezawa, *Surf. Sci.*, 1992, **261**, 342–348.
18 S. Venkatachalam and T. Jacob, *Phys. Chem. Chem. Phys.*, 2009, **11**, 3263–3270.
19 J. S. Jirkovský, I. Panas, S. Romani, E. Ahlberg and D. J. Schiffrin, *J. Phys. Chem. Lett.*, 2012, 315–321.
20 J. H. Scofield, *J. Electron Spectrosc. Relat. Phenom.*, 1976, **8**, 129–137.
21 *ASF Dataset* provided by SPECS, 2008.

22 G. C. Smith and A. K. Livesey, *Surf. Interface Anal.*, 1992, **19**, 175–180.
23 A. K. Livesey and G. C. Smith, *J. Electron Spectrosc. Relat. Phenom.*, 1994, **67**, 439–461.
24 R. W. Paynter, *J. Electron Spectrosc. Relat. Phenom.*, 2009, **169**, 1–9.
25 R. W. Paynter, *Surf. Interface Anal.*, 1999, **27**, 103–113.
26 C. Verdozzi, P. A. Schultz, R. Wu, A. H. Edwards and N. Kioussis, *Phys. Rev. B: Condens. Matter*, 2002, **66**, 125408.
27 A. R. West, *Solid state chemistry and its applications*, John Wiley & Sons, Chichester, 1984.
28 P. W. Atkins, *Physical Chemistry*, Oxford University Press, Oxford, 1990, p. 623.
29 M. Polcik, L. Wilde, J. Haase, B. Brena, D. Cocco, G. Comelli and G. Paolucci, *Phys. Rev. B: Condens. Matter*, 1996, **53**, 13720–13724.
30 J. Emsley, *The Elements*, Clarendon Press, Oxford, 1989.
31 J. Zemek, *Anal. Sci.*, 2010, **26**, 177–186.
32 S. Oswald and F. Oswald, *Phys. Status Solidi C*, 2007, **4**, 1817–1821.
33 S. Mróz, *Prog. Surf. Sci.*, 1998, **59**, 323–330.
34 B. Good, G. H. Bozzolo and P. B. Abel, *Surf. Sci.*, 2000, **454–456**, 602–607.
35 M. Okada, K. Moritani, T. Fukuyama, H. Mizutani, A. Yoshigoe, Y. Teraoka and T. Kasai, *Surf. Sci.*, 2006, **600**, 4228–4232.
36 H. C. Poon, B. C. Khanra and T. S. King, *Phys. Rev. B: Condens. Matter*, 1993, **47**, 16494–16498.
37 V. Soto-Verdugo and H. Metiu, *Surf. Sci.*, 2007, **601**, 5332–5339.
38 K. J. J. Mayrhofer, K. Hartl, V. Juhart and M. Arenz, *Angew. Chem., Int. Ed.*, 2009, **48**, 3529–3531.
39 K. J. J. Mayrhofer, K. Hartl, V. Juhart and M. Arenz, *J. Am. Chem. Soc.*, 2009, **131**, 16348–16349.